Quantitative assessment of morphology and sub-cellular changes in macrophages and trophoblasts during inflammation

RAJWINDER SINGH,[1,2,6] VISHESH DUBEY,[1,3,6] DEANNA WOLFSON,[1] AZEEM AHMAD,[1] ANKIT BUTOLA,[3] GANESH ACHARYA,[4] DALIP SINGH MEHTA,[3] PURUSOTAM BASNET,[5,7] AND BALPREET SINGH AHLUWALIA[1,4,8]

[1]*Department of Physics and Technology, UiT The Arctic University of Norway, Tromsø 9037, Norway*
[2]*Cell Biology and Biophysics Unit, European Molecular Biology Laboratory, Heidelberg, Germany*
[3]*Department of Physics, Indian Institute of Technology Delhi, Hauz Khas, New Delhi 110016, India*
[4]*Department of Clinical Science, Intervention and Technology Karolinska Univ. Hospital, Sweden*
[5]*Womeńs Health and Perinatology Research Group, Department of Clinical Medicine, UiT The Arctic University of Norway and Department of Obstetrics and Gynecology, University Hospital of North Norway, Tromsø, Norway*
[6]*Author with equal contribution*
[7]*purusotam.basnet@uit.no*
[8]*balpreet.singh.ahluwalia@uit.no*

Abstract: In pregnancy during an inflammatory condition, macrophages present at the feto-maternal junction release an increased amount of nitric oxide (NO) and pro-inflammatory cytokines such as TNF-α and INF-γ, which can disturb the trophoblast functions and pregnancy outcome. Measurement of the cellular and sub-cellular morphological modifications associated with inflammatory responses are important in order to quantify the extent of trophoblast dysfunction for clinical implication. With this motivation, we investigated morphological, cellular and sub-cellular changes in externally inflamed RAW264.7 (macrophage) and HTR-8/SVneo (trophoblast) using structured illumination microscopy (SIM) and quantitative phase microscopy (QPM). We monitored the production of NO, changes in cell membrane and mitochondrial structure of macrophages and trophoblasts when exposed to different concentrations of pro-inflammatory agents (LPS and TNF-α). *In vitro* NO production by LPS-induced macrophages increased 22-fold as compared to controls, whereas no significant NO production was seen after the TNF-α challenge. Under similar conditions as with macrophages, trophoblasts did not produce NO following either LPS or the TNF-α challenge. Super-resolution SIM imaging showed changes in the morphology of mitochondria and the plasma membrane in macrophages following the LPS challenge and in trophoblasts following the TNF-α challenge. Label-free QPM showed a decrease in the optical thickness of the LPS-challenged macrophages while TNF-α having no effect. The vice-versa is observed for the trophoblasts. We further exploited machine learning approaches on a QPM dataset to detect and to classify the inflammation with an accuracy of 99.9% for LPS-challenged macrophages and 98.3% for TNF-α-challenged trophoblasts. We believe that the multi-modal advanced microscopy methodologies coupled with machine learning approach could be a potential way for early detection of inflammation.

1. Introduction

Macrophages play an important role in immune response, tissue development, remodelling and repair [1,2]. They are generally classified into two categories depending on how they respond to the various environmental signals: classically activated macrophages (M1) and alternatively

activated macrophages (M2). M1 macrophages are stimulated by the virus infections, endotoxin (LPS) or some cytokines e.g. TNF-α, INF-γ, etc. Important cytokines, such as IL-1, IL-6, IL-12 and TNF-α are released in response. M2 macrophages help in the tissue remodelling and repair and are characterised by the release of the cytokines such as IL-2β and IL-10 [3,4]. In a pregnant woman placental decidua contains 20-30% macrophages of the total population of the leukocytes. During peri-implantation period, the decidual macrophages are inclined towards M1 phenotype. Their profile predominantly shifts towards M2 macrophage phenotypes during the pregnancy. Macrophages play important role in the spiral artery remodelling and the trophoblast invasion by clearing the apoptotic cells in the decidua [5,6].

Better communication between the fetal trophoblast and maternal immune cells is very important for the successful outcome of a pregnancy. The trophoblast, just like an innate immune cell, expresses pattern recognition receptors (PRR) that act as 'sensors' of the surrounding environment [7]. Through PRR, the trophoblast can recognize the presence of pathogens, dying cells and damaged tissue [8]. Upon recognition, the trophoblast secretes certain cytokines that in turn, will act upon the immune cells within the decidua (i.e. macrophages, T regulatory cells, NK cells), recruiting and educating them to work together in support of the growing fetus [7–9]. A viral or bacterial infection may perturb the harmony of the cross-talk between macrophages and trophoblasts which might lead to various pregnancy complications [10]. One of the major pathogens causing these infections is gram negative bacteria. These bacteria colonise the genitourinary tract of women, where they continuously release an endotoxin called lipopolysaccharide (LPS). LPS is present on the outer membrane of the gram-negative bacteria which induces inflammation by stimulating the immune system, particularly macrophages [11]. Classically activated macrophages produce TNF-α and nitric oxide (NO) in abundance which has been linked with pre-eclampsia, preterm delivery and early abortion [12,13].

Several studies have been conducted to understand the mechanisms of inflammation in macrophages and trophoblasts following stimulation with various cytokines. However, we have insufficient information about the effect of LPS and other cytokines released in its effect on the morphology of these cells at the sub-cellular level. Plasma membrane play an important role during inflammation. PRR are generally expressed on the plasma membrane and after recognising any foreign molecule, signalling cascade is initialised which instructs a cell to produce cytokines. In addition to the plasma membrane which is the first point of contact to inflammatory agents, mitochondria are another important sub-cellular organelle responsible for generating energy and thus well-being for the cell. Mitochondria produces reactive oxygen species (ROS) continuously during respiration [14]. In pathological state ROS can be overproduced and thus can cause oxidative stress (OS) [15]. OS can lead to mitochondrial swelling and initiate an apoptotic cascade [16,17]. Superoxide radical ($O_2\cdot^-$) may also react with NO produced during infection to produce a toxic substance peroxynitrite ($ONOO^-$) damaging the cells [18]. There have been few studies carried out using electron microscopy which suggest that the mitochondrial morphology of trophoblasts is altered under pathological conditions [19,20], but these studies are limited to fixed cell due to incompatibility of electron microscopy with live cell imaging. So far, to the best of our knowledge super-resolution microscopy has not been explored for studying inflammation in live macrophages and trophoblasts. Therefore, the study of plasma membrane and mitochondria is crucial to mark the changes during inflammation. Many important details in the inflammation-related sub-cellular processes in these cells could have not been observed due to the limited spatial resolution of conventional fluorescence microscopy systems. Moreover, multi-modal imaging complemented with the chemical analysis are required to obtain better understanding of the inflammation related changes in macrophages and trophoblasts.

Structured illumination microscopy (SIM) is a wide-field super resolution optical microscopy technique having the twice resolution enhancement in all the three axis compared with the conventional optical microscopes [21]. Among the existing super-resolution optical microscopy

techniques, SIM offers advantage of relatively high-speed, three-dimensional imaging and most importantly compatible for the live cell imaging [21,22]. Recently, super-resolution imaging of three different sub-mitochondrial regions of living cells is reported using 3D SIM with a resolution of the order of 100-130 nm [23]. SIM can therefore be used to visualize and to quantify the change in the mitochondrial morphology when treated with different pro-inflammatory agents. Additionally, SIM is also compatible with wide range of conventionally used bright and stable fluorophores making it popular choice for imaging and optical sectioning of live biological cells [22,24]. SIM is fluorescence-based technique and therefore requires exogenous labelling agents for imaging cells. In label-free optical imaging, quantitative phase microscopy (QPM) is a popular technique for the quantitative analysis of live biological specimens [25]. QPM techniques are capable to quantify various parameters associated with biological specimen, such as cell dynamics (fluctuations in cell thickness and/or RI), cell morphology and cell dry mass (non-aqueous content) [25–28]. Digital holographic microscopy (DHM) is one of the interferometric QPM techniques to extract the quantitative information of the live cell [27]. It is very useful technique for the single cell analysis with ease of operation and compatibility [28,29]. In connection with vigorous algorithms of numerical reconstruction of interferograms for data measurement, DHM provides a fascinating window in modern microscopy for quantitative analysis of the specimen. In addition, single shot DHM techniques can be used for the measurement of dynamic fluctuation of the live cells [30]. The 3D cell shape can be obtained from quantitative phase which having information about the integral cell refractive index and the cell thickness [27]. This enables to determine various parameters of the cells such as volume, surface area, sphericity, etc [27,31], which could be studied as bio-marker of cell inflammation. Several machine learning approaches were also aided to QPM in order to interpret large-scale and high-dimensional data for classification and diagnosis [27,32,33].

In this work, we have applied different optical modalities for the observation of various morphological changes on cellular and sub-cellular levels in macrophages and trophoblasts after inducing inflammation with LPS or TNF-α at different concentrations. We observed the effects of various concentrations of LPS or TNF-α on NO production, cell membrane and mitochondria of macrophages and trophoblasts at different time intervals. The inflammatory responses of the macrophages and trophoblasts were observed by measuring the production of nitric oxide (NO), changes in cell membrane and mitochondrial structure when exposed to different concentration of pro-inflammatory agents. We measured a 22-fold increase in LPS-induced *in vitro* NO production by macrophages as compared to controls, whereas no significant NO production after TNF-α challenge. While trophoblasts did not produce significant amount of NO following either LPS or TNF-α challenge under similar conditions as with macrophages. The morphological changes in the plasma membrane and mitochondria were observed under super-resolution SIM microscopy. A significant change in the morphology of mitochondria and plasma membrane is observed in macrophages following LPS challenge and in trophoblasts following TNF-α challenge. QPM suggested a decrease in the optical thickness of the LPS-challenged macrophages, while TNF-α having no effect. The vice-versa is observed for the trophoblasts in label-free manner. Further, we have applied support vector machine (SVM) based algorithm on the morphological and texture parameters extracted from phase images for the classification of control and inflammation state [34,35]. The results suggest that these techniques together provide the clear visual and quantitative insights about the morphological and sub-cellular level changes in macrophages and trophoblasts in normal and pathological conditions. The basic information obtained in the present study could be useful for the treatment strategy in the future for the cases of the infection and inflammation in pregnancy.

2.   Materials and methods

2.1.   Materials

RPMI (Roswell Park Memorial Institute) 1640 medium (#R8758), LPS (#L2880), TNF-α (#T5944), sulphanilamide (#S9251), naphthalene diamine dihydrochloride (#N91250) and Dulbecco's PBS (Phosphate-buffered saline #D8537) were bought from Sigma-Aldrich, St Louis, MO, USA. Agilent 8453 UV-Visible Spectrophotometer, Agilent Technologies, Santa Clara, USA. FALCON 24-Well cell culture plates, Corning Incorporated, New York, USA. Zeiss standard binocular microscope, Carl Zeiss, West Germany with 10X and 40X objective lenses. CellMask Green (CMG) (#C37608), MitoTracker Green (MTG) (#M7514) and live cell imaging solution (#A14291DJ) were bought from Thermo Fisher Scientific (Waltham, USA). #1.5, 25 mm round coverslips (#631-0172) were bought from VWR international. Human fibronectin purified from human plasma by affinity chromatography on Gelatin Sepharose 4B was a kind gift from Vascular Biology Research Group, Department of Clinical Medicine, UiT-The Arctic University of Norway. Commercial OMX 3D-SIM v4 blaze system (GE Healthcare, USA) and custom build quantitative phase microscopy system are used for SIM and QPM, respectively, at Optical Nanoscopy Lab, UiT-The Arctic University of Norway.

2.2.   Cell culture

Macrophages (RAW 264.7, murine cell lines) and trophoblasts (HTR-8/SVneo, human cell lines) were used in the experiments and bought from ATCC. Cell culture was carried out in laboratory of Women's Health and Perinatology Research group, UiT-The Arctic University of Norway. Both cell lines were cultured separately in a humidified atmosphere of 95% air and 5% CO_2 at 37 °C with glutamine containing RPMI-1640 medium supplemented with 10% fetal bovine serum and antibiotics (penicillin and streptomycin). The cells were subcultured every 2-3 days by transferring the cells to the next passage and were utilized for experiments at 80-90% confluency.

2.3.   Measurement of NO production

For NO measurements, 1×10^5 cells/ml were transferred to each well of the 24-well culture plates. The cells could stabilize and adhere for 24 h in an incubator at 37° C and 5% CO_2. The cells were then treated with three different concentrations of LPS (0.1 μg/ml, 1 μg/ml, 10 μg/ml). The production of NO released in the medium were measured spectrophotometrically in terms of nitrite formation by Griess reagent [36,37] at 540 nm using $NaNO_2$ as the standard. The measurements were performed in triplets at different time points as the result shown in Fig. 1. Similar plan was adopted to measure the NO after TNF-α challenge at three different concentrations (10 pg/ml, 100 pg/ml and 1000 pg/ml).

2.4.   Labelling and super resolution imaging of macrophages and trophoblasts

We optimised the labelling protocol for staining plasma membrane and mitochondria for both cell types using CellMask Green (CMG) and MitoTracker Green (MTG), respectively. We found that the concentration 1:1000 of CMG and 60 nM of MTG is optimum for good reconstruction of SIM images for both the cell types. Both dyes are excited by the same wavelength ($\lambda_{ex} = 488$ nm). For labelling plasma membrane, live cells on the coverslips were washed once with RPMI and then CMG (1:1000) is applied and sample is incubated for 10 min. For mitochondria labelling, live cell sample is washed once with RPMI and then incubated with MTG (60 nM) for 30 min. Then the sample is washed with RPMI thrice and mounted in imaging solution. For SIM imaging, cells were seeded on #1.5 coverslips (170 μm thick) the day before imaging and were incubated. Next day cells were challenged with an inflammatory agent and data were acquired at 2 h, 4 h, 6 h and 24 h time points. Cells were imaged at these time-points on SIM afterwards.

3D-SIM images of macrophages and trophoblasts were acquired at room temperature (T = 23 °C) and within 1 h after taking out of the incubator on a commercial structured illumination microscope (DeltaVision|OMXv4.0 BLAZE, GE Healthcare). All the images were acquired using 488 nm laser (Fiber coupled laser with output power of 65 mW) with power set to either 10% or 31.5%. The actual power reaching at sample plane is less than rated value as there is a loss in the power going through the optics. The images shown in this study are the projected image of z-section stacks. Each z-section is 0.125 µm thick and the thickness of samples imaged was kept between 1.2-2.5 µm. Exposure time was generally kept between 10-40 ms. After acquisition, images were reconstructed using the SoftWorX package from GE Healthcare.

2.5. *Quantitative phase imaging of macrophages and trophoblasts*

For QPM measurements, the cells were seeded in PDMS chambers located on reflecting silicon slides. Samples were incubated for 24 h and later cells were divided into two batches (a) control and (b) challenged with inflammatory agents for the experiment. For time course imaging, cells from same cell culture passage were seeded on different silicon slides. After 24 h incubation, slides were divided randomly into five batches. One was kept as a control and four were challenged with inflammatory agents to be imaged at 2 h, 4 h, 6 h and 24 h time points.

A Linnik type DHM setup was used for the imaging of the biological samples [27,29]. Unlike to SIM microscopy, this technique does not require any labelling agent to quantify the morphological features [38]. The details of the set up can be found elsewhere [25,27,28]. A 60 × microscope objective (NA = 1.2) is used for the imaging of the control and inflamed live cells. Imaging was performed at room temperature and under normal atmospheric conditions. For time course imaging, one slide was chosen at random from the batches prepared to be imaged at a particular time point and then discarded. He-Ne laser @632.8 nm was used to illuminate the object and record the off-axis holograms with help of CMOS camera (Hamamatsu ORCA-Flash4.0 LT, C11440-42U). These images were used further for the post processing. Fourier transform analysis was used to extract the phase delay induced by the specimen, which represents the average refractive index and thickness of specimen at all spatial points [25,27]. The experiment was repeated several times on each set of the sample.

3. Results and discussion

3.1. *NO production measurements*

The response of macrophages and trophoblasts on NO production was studied after challenging them with various concentrations (0.1 µg/ml, 1 µg/ml, 10 µg/ml) of LPS and TNF-α (10 pg/ml, 100 pg/ml and 1000 pg/ml). NO produced has physiological relevance. The range of concentration (dosage) used both for LPS (NO concentration) and TNF-α had been previously reported in the literature for inflammation related studies [39–42]. Various studies have shown that in preeclamptic women, the concentration of NO in serum can vary from 16 µM to 39 µM. In normal human serum, TNF-α is approximately 10 pg/mL and higher under inflammatory conditions [43]. Kuperminc et.al found 210 pg/ml of TNF-a in the sera of preeclamptic women as compared to 65 pg/ml in controls [42]. We performed measurement at different time points (0 h, 4 h, 8 h, 12 h, 24 h). After inflammation induced by LPS, the macrophages produce a large amount of NO after 24 h as shown in Fig. 1(a1). It can be observed from Fig. 1(a1) that the challenged cells already started producing NO compared with control, but they were below the detection limit so the results up to 4 h are not conclusive. After 8 h, the macrophages produce a significant amount of NO to be detected. The maximum increase in the NO production is seen between 12 h-24 h. An increase in the NO production was expected and is in accordance with the previous studies [44,45]. Figure 1 demonstrates that the concentration of NO produced by macrophages even after 24 h upon challenging with various concentrations of LPS (0.1, 1, and 10 µg/mL)

Fig. 1. The production of NO by macrophages and trophoblasts after challenging with two inflammatory agents. (a1) macrophages and (a2) trophoblasts challenged with various concentrations LPS, (b1) macrophages and (b2) trophoblasts following TNF-α challenge at various concentrations. Bar graph shows the mean value (+S.D.) of three experiments. Considerable amount of NO was produced only in case of macrophages stimulated by LPS. The horizontal red line shows the limit of significant amount of NO production.

remain below or within the physiological range. In contrast, trophoblasts did not produce any significant amount of NO even after 24 h following LPS challenge as shown in Fig. 1(a2). Further, macrophages and trophoblasts were challenged with different concentrations of TNF-α (10 pg/ml, 100 pg/ml and 1000 pg/ml) and measured the corresponding amount of NO production in the cell culture media. Both macrophages and trophoblasts did not produce any significant amount of NO production even after 24 h of stimulation as shown in Fig. 1(b1)–(b2). Some values are above the significant amount of NO production, but the standard deviations for these readings are also large. Some negative values in the results might be due to the blank error.

In Table 1, we have listed the production of NO by macrophages and trophoblasts after inducing by the inflammatory reagents i.e. LPS and TNF-α. Only LPS challenged macrophages produced NO after 8 h of inflammation and remained maximum after 24 h. We could not measure any significant amount of increased NO production from trophoblast after LPS treatment. TNF-α could not induce the NO production to macrophages as well as trophoblasts. The red boxes of the table show the time point of the inflammation where the significant amount of NO is produced by cells and green boxes of the table showing the no significant level of NO production.

Table 1. Nitric oxide measurement results obtained from Griess method for LPS and TNF-α challenged macrophages and trophoblasts for different time points

	LPS Challenged					TNF-α challenged				
	0h	4h	8h	12h	24h	0h	4h	8h	12h	24h
Macrophages	-	-	+	+	+	-	-	-	-	-
Trophoblasts	-	-	-	-	-	-	-	-	-	-

3.2. SIM imaging of the cell membrane and mitochondria

To detect the changes at cellular and sub-cellular level during inflammation in macrophages and trophoblasts, SIM imaging is performed to obtain the super-resolved images of cell membrane and mitochondria. Initially, both the macrophages and trophoblasts were challenged with LPS (1 μg/ml) and TNF-α (1000 pg/ml) for 24 h. The plasma membrane and mitochondria were labelled with Cell Mask Green (CMG) and MitoTracker Green (MTG), respectively. Both dyes are excited by the same wavelength ($\lambda = 488$ nm). Cell Mask, is an amphipathic molecule containing a lipophilic part for membrane loading and a negatively charged dye for membrane anchoring. The plasma membrane of the cells were imaged with SIM imaging. The results show a drastic change in cell membrane morphology of LPS-challenged macrophages and TNF-α-challenged trophoblasts compared to the control cells as shown in Fig. 2. Figure 2(a) shows the control macrophages with defined boundaries and villi-like projections on the plasma membrane while Fig. 2(b) show the spreading and the membrane disintegration after inflammation. Figure 2(c)-(d) show the images of plasma membrane of control and TNF-α challenged trophoblasts. After inflammation, the cell membrane boundaries are disintegrated and the filopodia are less in numbers as compared to controls.
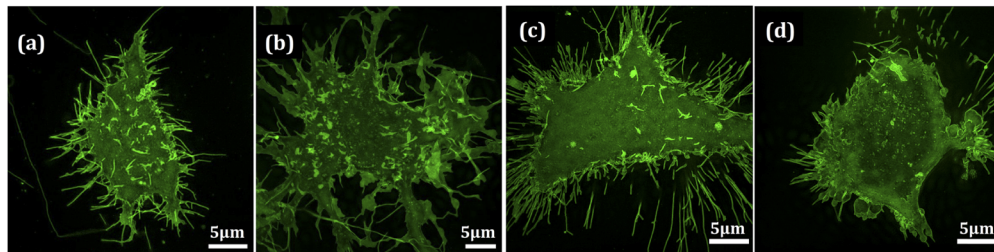
Fig. 2. 3-D projected images of plasma membrane labelled with CMG (λex = 488 nm) of (a) control and (b) LPS-challenged macrophages. Similar results obtained from (c) control and (d) TNF-α challenged trophoblasts. Comparing (a) vs. (b) and (c) vs. (d), it is observed clearly that the cell membrane integrity is lost with reduced number of filopodia after inflammation.

In addition to the cell membrane which is the first point of contact to inflammatory agents, mitochondria are another important sub-cellular organelle responsible for generating energy. The small size of mitochondria limits its visualization using diffraction limited optical microscope. Hence, super-resolution SIM imaging can reveal the changes in the morphology of mitochondria, especially in a live cell. Macrophages stimulated with LPS show different mitochondrial morphology as compared to the control cells. Figure 3 depicts the comparison between the mitochondrial morphology of control, LPS-challenged and TNF-α challenged macrophages. Figure 3(b) suggest that the mitochondria appear to be fragmented, round and shorter in LPS-challenged macrophages compared with control. Further, Fig. 3(e)-(g) show the magnified images of the mitochondria of selected region of Fig. 3(a)-(c). Contrarily, it was found that TNF-α challenge does not produce any remarkable change in the morphology of the mitochondria comparing to control. Further, we also performed statistical analysis on these mitochondrial images to visualize the changes due to inflammation. The quantification of mitochondrial number and footprint area was done using Mitochondrial Network Analysis (MiNA) Single Image macro [46]. We have quantified the counts of mitochondria and their footprint area. The footprint is defined as the total area covered by mitochondria (from SIM images) after separating from the background in the image. It is the number of pixels in the image containing information of the mitochondria multiplied by the area of a pixel, which is pre-calibrated. A total of 36, 33 and 40 cells for control, LPS challenge and TNF-α challenge macrophages were used to perform

statistical analysis as shown in Fig. 3(d), (h). Mitochondria counts in LPS challenged macrophages increases while TNF-α does not affect it. Interestingly the footprint of the mitochondria is also increased after LPS challenge macrophages while TNF-α challenge does produce any significant changes in the mitochondrial morphology of macrophages.
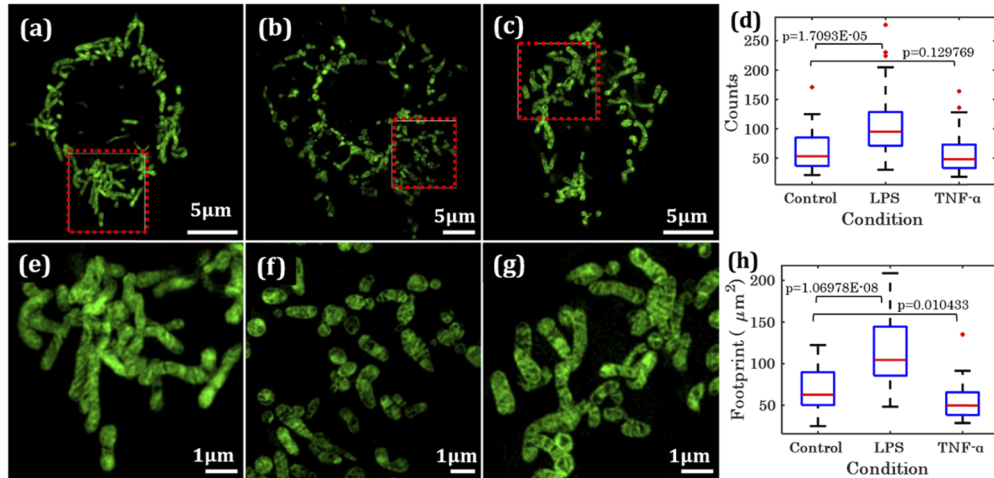

Fig. 3. 3-D projected SIM images of the mitochondria labelled with MTG (λex = 488 nm) in (a)-(c) control, LPS-challenged and TNF-α challenged macrophages, respectively. (e)-(g) are mitochondrial images of the region marked with red dotted box in (a)-(c). Mitochondria in LPS-challenged macrophages are shorter and rounded as compared to control and TNF-α challenge. (d), (h) show the variation in mitochondria counts and mitochondrial foot print area, respectively after LPS or TNF-α challenge in macrophages. * shows the outliers data points in dataset. The red horizontal line is median, the top and bottom edge of box show the 75th and 25th percentile of the distribution.

Similarly, the mitochondria of the LPS or TNF-α-challenged trophoblasts were also imaged and some representative images are depicted in Fig. 4. We did not observe significant changes on the morphology of mitochondria of trophoblasts while inducing LPS as compared to control (Figs. 4(a,b)). While, the morphology of the mitochondria changes when treated with TNF-α as shown in Fig. 4(c). The mitochondria appear fragmented and shorter in size compared to the control sample. Figure 4(e)-(g) show the magnified images of the mitochondria of selected region of Fig. 4(a)-(c), respectively. Figure 4(d),(h) provides the statistical analysis to show the variation using data of 33, 25 and 38 cells for control, LPS and TNF-α challenge trophoblasts, respectively. For trophoblasts, LPS does not produce any kind of morphological changes in mitochondria as observed from Fig. 4(d) while TNF-α changes the count of mitochondria after inflammation. Although, mitochondrial footprint seems to remain similar in all three cases as seen in Fig. 4(h). Further statistical analysis has been carried out with the SIM images to measure the experiment to experiment variation in the same class of the data. The result of statistical analysis is listed in the form of a table of all classes of data from 3 different experiments. The standard procedure for the statistical analysis can be found elsewhere [47]. The detailed information about all 3 experiments and their analysis is provided in appendix A. Table 2 provides an overview of the statistical analysis of 3 different experiments of the same kind of cell lines.

After confirming the direct inflammatory effects of LPS to macrophage and TNF-α to trophoblasts but not vice-versa, we performed experiments to visualize the rate of morphological changes during inflammation progress. This study also provides the information on initial stage of inflammation as detected by SIM. The results of SIM show that the changes in the morphology
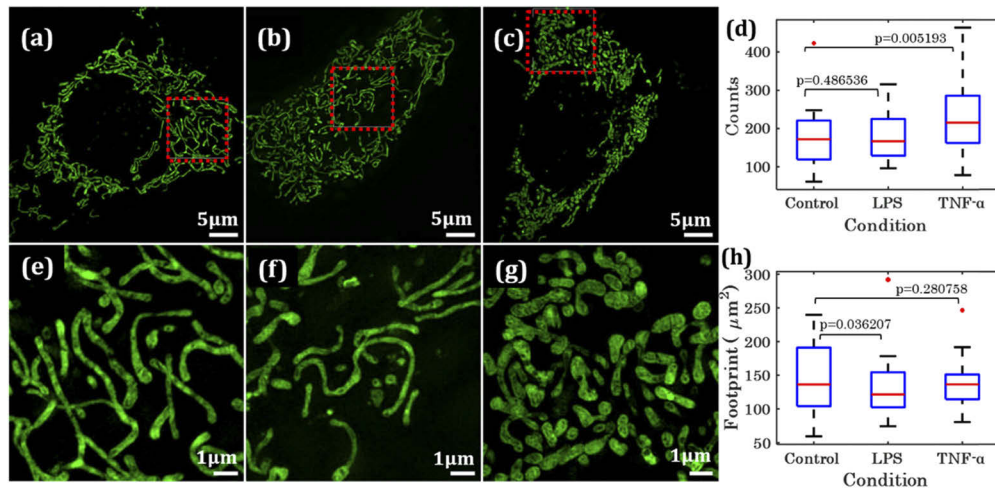
Fig. 4. 3-D projected SIM images of the mitochondria labelled with MTG (λex = 488 nm) in (a)-(c) control, LPS-challenged and TNF-α challenged trophoblasts, respectively. (e)-(g) are the region marked with red dotted box in (a)-(c). Mitochondria in TNF-α challenged trophoblasts are having different morphology as compared to control and LPS. (d),(h) show the change in mitochondria counts and mitochondrial foot print area, respectively after LPS or TNF-α challenge trophoblasts, respectively after LPS or TNF-α challenge. * shows the outliers data points in dataset. The red horizontal line is median, the top and bottom edge of box show the 75th and 25th percentile of the distribution.

Table 2. Statistical analysis of the data for different classes of macrophages and trophoblasts.

Class	Macrophages				Trophoblasts			
	Counts		Footprint area (μm^2)		Counts		Footprint area (μm^2)	
	mean	SD	mean	SD	mean	SD	mean	SD
Control	67.2	15.83	68.27	13.09	168.84	30.97	146.02	22.95
LPS challenged	117.63	6.68	130.38	26.95	171.84	12.28	132.33	21.55
TNF-α challenge	57.45	8.43	55.53	5.54	232.09	11.09	143.93	15.46

after 2 h inflammatory agent treatment, 20% of the cells are affected as shown in Fig. 5. This figure show the change in mitochondrial morphology of the macrophages for different time points of 2 h, 4 h and 6 h of inflammation (Figs. 5(b-d)) compared to control (Fig. 5(a)). Figure 5(e)-(h) show the magnified view of the selected region of the Figs. (a)-(d), respectively, which provide better visualization of the changes. From these images, it is observed that the morphology of the mitochondria is changing even after 2 h of inflammation compared to the control. It is interesting to note that at 2 h, NO measurements was not detected in LPS-induced macrophages, as shown in Fig. 1.

3.3. Quantitative phase imaging of macrophages and trophoblasts

The QPM of the macrophages and trophoblasts allow us to analyse the optical topography of the specimen and quantify different morphological parameters of the specimen. The quantitative phase information and the details of the morphological changes occurring in the specimen caused by LPS or TNF-α on the macrophages and/or trophoblasts could be a standard clinical application. Figure 6(a)-(c) show the phase images for control, LPS-challenged and TNF-α-challenged macrophages, respectively. From Fig. 6(b), it is observed that LPS exposed macrophages have
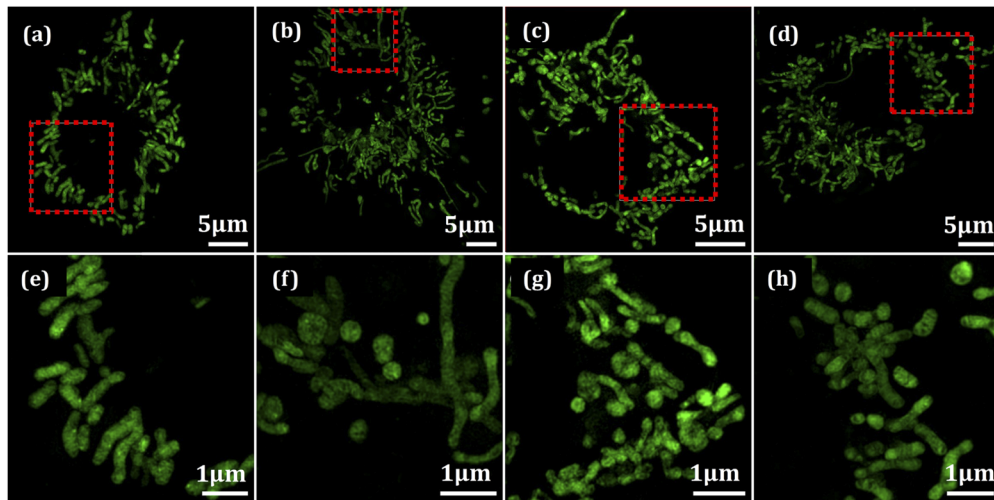
Fig. 5. Early time-point imaging of mitochondria of macrophages challenged with LPS. (a) Control; (b), (c) and (d): macrophages challenged with LPS after 2 h, 4 h and 6 h, respectively. (e)-(h) are the magnified image of selected areas of (a), (b), (c) and (d), respectively. The change in mitochondrial morphology can be observed after 2 h of inflammation compared to control.

changed cell morphology. The phase images clearly show that there is decrease in the maximum phase of LPS challenged macrophages as compared to the normal one. The phase image of cell maps the optical path length at each spatial point of the cell, which is a product of the cell thickness and refractive index contrast of the cells and the culture medium. Assuming the refractive index does not change significantly, the net decrease of the maximum phase suggests the thickness of the cell has decreased after LPS challenge. It can also be observed from Fig. 6(b) that there is an increase in the size of the cell after inflammation as also noticed in SIM images as shown in Fig. 2(b). Thus, the LPS challenged inflammation on macrophages makes the cell flatter (optically thin) and bigger in area. Contrary, TNF-α does not induce any changes in the phase images of the macrophages as shown in Fig. 6(c) where the phase values of the TNF-α-challenged cells are almost similar to normal one. Also, it does not induce any significant effects on the size of the cells.

We have studied the effects of these inflammatory reagents in detail by performing the experiment over different batches and passes of macrophages and trophoblasts and repeated several times (around 200 cells of each case). Figure 6(d) show the box plots of maximum phase of the macrophages challenged with different concentrations (0.1 µg/ml, 1 µg/ml and 10 µg/ml) of LPS. Results shows that as LPS concentration increased the phase values decrease. There is no change in the maximum phase (optical thickness) of the macrophages observed after challenging different concentrations (10 pg/ml, 100 pg/ml and 1000 pg/ml) of TNF-α as shown in Fig. 6(e). The concentration dependent experiment was performed after 24 h of incubation of the sample with inflammatory reagents. Further, the phase imaging at different time points for a fixed concentration of 1 µg/ml of LPS, show that the QPM system is capable to detect the minute changes in the morphology just after 2 h of LPS treatment as shown in Fig. 6(f). This is contrary, under similar condition, measurable quantity of NO production was observed only after 8 h of LPS-induced inflammation, see Table 1.

Similarly, the effect of various concentration of LPS (0.1 µg/ml, 1 µg/ml and 10 µg/ml) and TNF-α (10 pg/ml, 100 pg/ml and 1000 pg/ml) on the morphology of trophoblasts are also studied in detail using QPM. Figure 7(a)-(c) show the representative phase maps of control,
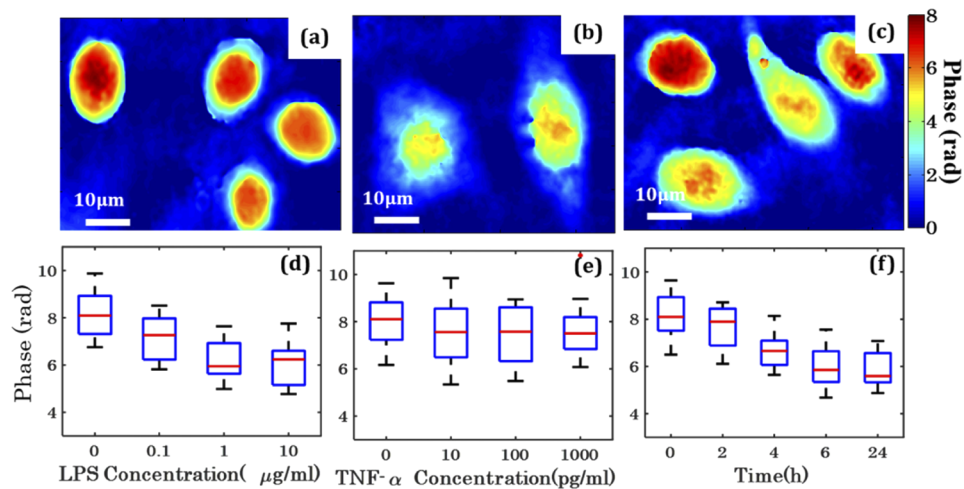
Fig. 6. Quantitative phase images of the macrophages and change in the phase map after LPS and TNF α induced inflammation. Figures (a)-(c) show the representative phase images of macrophages for control, LPS-challenged and TNF-α-challenged, respectively. Figures (d) and (e) show LPS and TNF-α concentration dependent change in the maximum phase of macrophages, respectively. Figure (f) shows the time dependent change in the maximum phase of macrophages after challenging with LPS (1 μg/ml). * shows the outliers data points in dataset.

LPS-challenged and TNF-α-challenged trophoblasts, respectively. It is observed from Fig. 7(b) that LPS does not change the trophoblasts morphology while TNF-α induces reduction of the maximum phase of trophoblasts as shown in Fig. 7(c). An increment in the cell size is observed after treatment with TNF-α which is otherwise not visible in LPS-challenged trophoblasts. Further, the concentration dependent experiment was performed after 24 h and the variation in the phase of trophoblast are also quantified as a function of concentration and shown in Fig. 7(d), (e). From the result of phase image and quantitative data, it can be concluded that LPS do not show direct effect on trophoblast while TNF-α affects trophoblasts by causing on reduction in the maximum phase (optical thickness) of the specimen. Figure 7(f) show the change in the phase of trophoblasts at different time points after inducing the 1000 pg/ml concentration of TNF-α. The results show that the QPM system is also capable of detecting the early stage changes in the morphology of the trophoblasts at initial time point of 2 h.

QPM provides the label-free imaging for the quantification of the effect of various inflammatory reagents as well as it is capable to detect the changes in the morphology of the cells after inflammation. These results have a good agreement with the outcomes of the SIM. QPM results contain the information about the change in the optical thickness distribution of the cells as well as various morphological parameters during inflammation. The quantification of these parameters can be helpful for the classification control and inflamed cells in very early stage. Therefore, exploiting machine learning, a support vector machine (SVM) [34,35] based classifier has been developed and trained with the outcomes of QPM results for the classification of the normal and inflamed cells.

3.4. Feature extraction and classification of control and inflamed cells

Application of machine learning tools to optical microscopy and medical imaging provided the new dimension. Single shot phase images acquired using QPM can be used to acquire large set of data without the need of extra-labelling step. This makes QPM an attractive route to
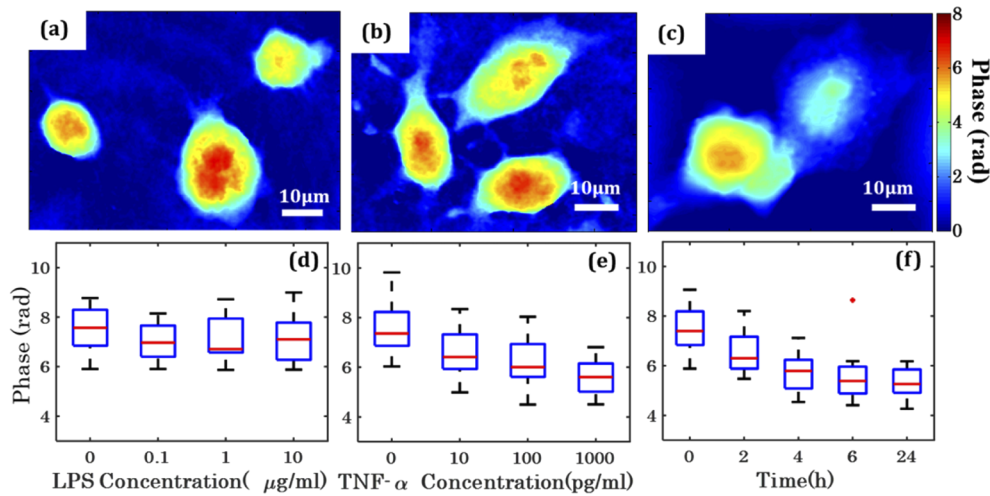
Fig. 7. Quantitative phase images of the trophoblasts and change in the phase map after LPS and TNF-α-induced inflammation. Figure (a)-(c) show the representative phase images of trophoblasts for control, LPS challenge and TNF-α challenge respectively. Figure (d) and (e) show LPS and TNF-α concentration dependent change in the maximum phase of trophoblast, respectively and (f) show time dependent change in the maximum phase of trophoblasts after inducing with TNF-α (1000 pg/ml). * shows the outliers data points in dataset.

explore with machine learning. To this end, a support vector machine (SVM) based classifier was developed for the classification of the inflamed macrophages and trophoblasts as the pathological cells comparing to normal healthy cells. As the focus is to predict early stage of infection, we measured the parameters of the cells with LPS treatment for macrophage and TNF-α treatment for trophoblast after 2 h. A total number of 200 cells of each condition were used for this study.

Several morphological and texture parameters were derived from the acquired phase images of control and inflamed macrophages or trophoblasts at 2 h time point. The steps and details of cell segmentation for feature extraction from phase images were discussed in the appendix B. We observed that TNF-α did not induce the cascades of inflammation in macrophages and similarly, LPS does induce any direct cascades of inflammation in trophoblasts. Therefore, for the classification of control vs. inflamed cells, we considered only two cases (a) control vs. LPS-challenged macrophages and (b) control vs. TNF-α-challenged trophoblasts. We have extracted number of morphological parameters such as optical thickness (OT), area (A) and volume (V) as well as number of texture parameters (such as mean, variance, entropy, kurtosis and skewness) of phase distribution over the cell structure, and the dataset can be found on OSA figshare [42]. These parameters are extracted in order to measure the deformation in the morphology and phase distribution of the specimen after inflammation. In Table 3 we have listed morphological and texture parameters of the control and inflamed macrophages and trophoblasts for the classification.

The SVM algorithm is a binary classifier which can detect the inflammation in macrophages and trophoblasts. The receiver operating characteristic (ROC) curve is calculated for better classification at early time points. We have used only non-correlated morphological (max phase, OT and area) and texture (mean, variance, entropy, kurtosis and skewness) parameters as input variables and the actual state of the inflammation as response variable i.e. 0 for control and 1 for inflammation state. For the training of the classifier, 60% of the total 400 cells are used by random selection and rest 40% are used as testing data. The sensitivity, specificity and area

Table 3. The morphological and texture parameters for controls vs. inflamed macrophages (1 µg/ml concentration of LPS) and trophoblasts (1000 pg/ml concentration of TNF-α) at 2 h of time point.

Parameter	Definition	Macrophages		Trophoblasts	
		Control	2 h	Control	2 h
Max Phase (rad)	ϕ	8.247	7.161	7.695	6.94
OT (µm)	$OT = \phi(x,y) * \lambda/4\pi$	0.432	0.326	0.412	0.352
Area (µm²)	$dS = dxdy\sqrt{1 + G_x^2 + G_y^2}$	377.49	661.02	523.67	806.5
Volume(fl)	$V = \iint OT(x,y)dxdy$	49.91	51.98	57.372	119.432
Mean	$\frac{1}{N}\sum_{i=1}^{N}\phi_i$	5.063	3.622	4.099	3.31
Variance	$\frac{1}{N}\sum_{i=1}^{N}(\phi_i - \mu)^2$	6.059	2.727	4.195	2.687
Entropy	$-\sum_{i=1}^{N}p(\phi_i)log_2 p(\phi_i)$	1.389	1.615	1.011	1.787
Kurtosis	$\frac{1}{N}\sum_{i=1}^{N}\left[\frac{(\phi_i-\mu)}{\sigma}\right]^4 - 3$	1.909	1.706	1.893	1.831
Skewness	$\frac{1}{N}\sum_{i=1}^{N}\left[\frac{(\phi_i-\mu)}{\sigma}\right]^3$	−0.345	0.056	0.111	0.142

under curve (AUC) is calculated to measure the accuracy of the classifier. Figure 8 show the ROC curve for the classification of control vs. inflamed macrophages or trophoblasts. The accuracy for the classification of LPS-challenged macrophages is 99.9% as shown in Fig. 8(a). For TNF-α-challenged trophoblasts, the accuracy of the classifier is achieved 98.3% as depicted in Fig. 8(b).
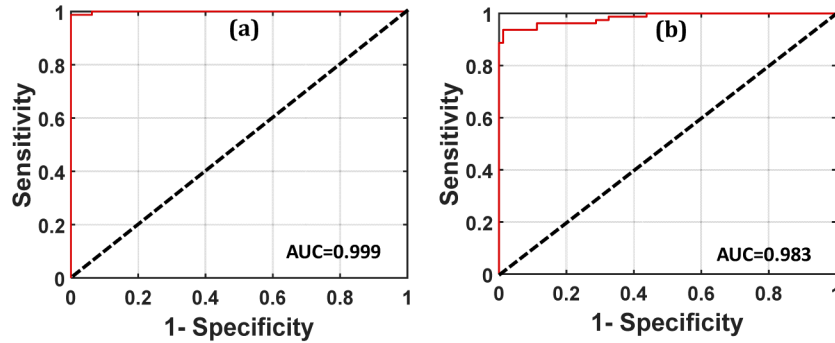
Fig. 8. ROC curve for testing dataset for the classification of controls vs. inflamed (a) macrophages or (b) trophoblasts. All the dataset for inflamed cells used for the classification are at 2 h time point. See data-1 and data-2 for raw data set [48].

We have also used t-SNE (T-distributed Stochastic Neighbor Embedding) method for better visualization of the distribution of data [49]. The results of t-SNE are provided in appendix C. The raw data set is also available for the readers on OSA figshare and can be downloaded using link provided in Ref. [48]. The results of t-SNE confirms that the data set is well separable and having good accuracy for the classification of control and inflammation states as shown in Fig. 8.

4. Conclusion

In present study, we have quantified the cellular and sub-cellular morphological and functional changes in macrophages and trophoblasts in response to two inflammatory agents i.e. LPS and TNF-α. We observe that the LPS induces significantly large amount of NO production

in macrophages which in turn also affects the morphology of mitochondria and the plasma membrane as depicted by SIM images. It also affects either the thickness of the cell or the cellular content (RI) as revealed by QPM results. Contrarily, using high-resolution SIM microscopy, it was found that macrophages undergo morphological changes following LPS-challenge. However, another inflammatory agent TNF-α did not show any direct effect to macrophages. Particularly for trophoblasts, no significant amount of NO produced even after inflammation induced by both inflammatory agents (LPS or TNF-α) because of iNOS presence, however, the cellular and sub-cellular changes can be easily detected and quantified using SIM and QPM. Through SIM and QPM, it was also found that the effect on the morphology changes of macrophages and trophoblasts can be observed following just 2 h of incubation with LPS or TNF-α, respectively, whereas the NO production in LPS-induced macrophage could not be detected at 2 h. SIM results suggest that the damage in the plasma membrane was more prominent than in mitochondria at early time-points compared with control samples, and the size of cells started to increase following only 2 h of incubation. The statistical analysis of SIM images of mitochondria suggests that the TNF-α does not produce a detectable level of inflammation in macrophages directly while LPS changes the morphology at cellular and sub-cellular level. Similarly, LPS does not produce detectable level of inflammation in trophoblasts while TNF-α does. QPM results show that the morphology of LPS-challenged macrophages or TNF-α-challenged trophoblasts are drastically changing. The effect of different concentration of LPS or TNF-α on the morphology of macrophages or trophoblasts are also quantified with the phase imaging of the cells. Interestingly, we have demonstrated that QPM could detect the cellular changes in inflamed macrophages even before the production of nitric oxide. QPM detected the changes in the morphology just after 2 h of inflammation, (Fig. 6(f)) while under similar condition, measurable quantity of NO production was observed only after 8 h (Table 1).

Super-resolution SIM and QPM techniques can be applied directly to live-cell, a few cells are sufficient to detect and distinguish the pathological conditions, multiple cell types can be analysed at the same time, and the state of inflammation can be detected quantitatively in the early stage. Multi-modal advanced microscopy techniques coupled with machine learning could be the useful tools to evaluate sub-cellular mechanisms associated with inflammation-mediated pregnancy complications. Fetal development depends on the proper functioning of trophoblasts cells of placenta. On the course of pregnancy and fetal development, generally mother is exposed to different kind of infections and inflammations. However, methods of studying the mechanisms how inflammation could disrupt the function of trophoblast cells are scarce. Therefore, it is of interest to develop tools that can elucidate behavior of trophoblast cells when exposed to inflammatory agents and that of immune cells which are directly involved in modulating inflammatory responses. In the current manuscript we present a tool that can structurally and quantitatively map out the trophoblast cell behavior under inflammatory stress. We have however used murine and human cell lines to establish the imaging methodology and to investigate the usefulness of SIM and QPM for inflammation studies. In future, more experiments are necessary to draw clinically relevant biological conclusion using human cell lines or primary cells wherever possible. Nevertheless, our findings clearly demonstrate that two different types of cells exposed to same type of inflammatory molecules for the same amount of time may respond differently at subcellular level with distinct effects on cell organelles. These variations at the sub-cellular level can be visualized structurally and quantified using SIM and quantitative phase microscopy. Here, we demonstrated that a simple SVM based classifier can achieve an accuracy of 99.9% for LPS-challenged macrophages and 98.3% for TNF-α-challenged trophoblasts.

Appendix A: Statistical assessment of SIM images for experiment to experiment variation

Number of experiments were performed to complete the study; therefore, we have performed the statistical analysis to measure the variation in experiment to experiment data as listed in Table 2. It is important to repeat experiment several times to ensure that the results are reproducible. We have performed statistical analysis on data from 3 different experiments and due to inherent biological variation, it is expected that variability between the mean of experimental data is high in some cases [47,50]. The results for macrophages and trophoblast are shown in Figs. 9 and 10.
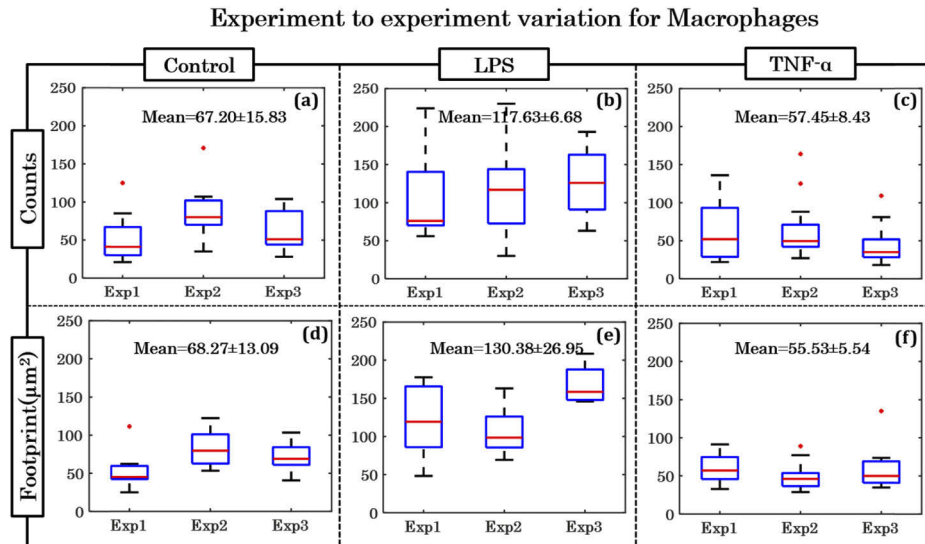
Fig. 9. Statistical analysis for measurement of experiment to experiment variation in mitochondria counts and their footprint area for 3 different set of experiments. Data for each experiment (Exp 1 to 3) are shown as a box plot. Fig. (a-c) show the experiment to experiment variation in mitochondrial counts for control, LPS challenged and TNF-α challenged macrophages, respectively. The red horizontal line is median, the upper bar equals the 75th percentile and the bottom bar equals the 25th percentile of the distribution. Fig (d-f) show the experiment to experiment variation in footprint area of mitochondria for control, LPS challenged and TNF-α challenged macrophages.
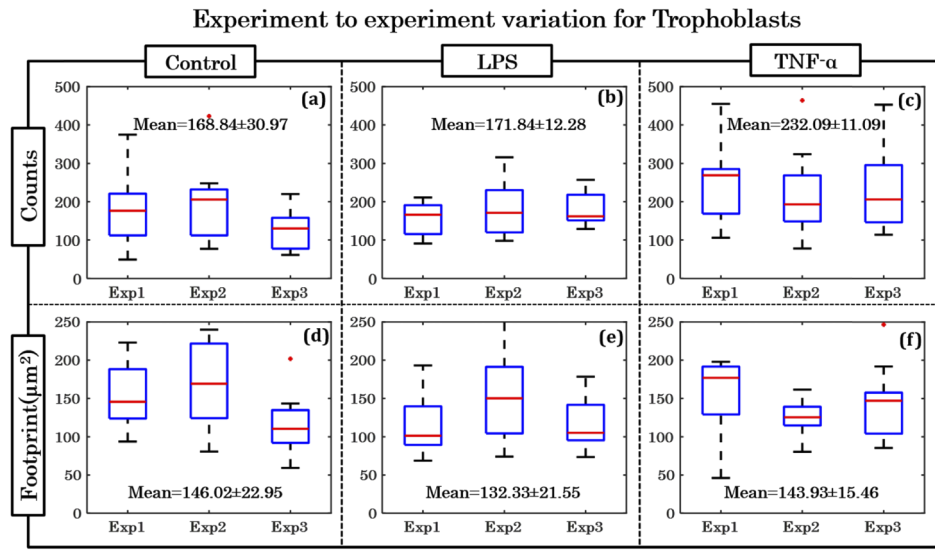
Fig. 10. Statistical analysis for measurement of experiment to experiment variation in mitochondria counts and their footprint area for 3 different set of experiments for trophoblasts. Data for each experiment (Exp 1 to 3) are shown as a box plot. Fig. (a-c) show the experiment to experiment variation in mitochondrial counts for control, LPS challenged and TNF-α challenged trophoblasts, respectively. The red horizontal line is median, the upper edge of box equals the 75th percentile and the bottom edge corresponds to 25th percentile of the distribution. Fig (d-f) show the experiment to experiment variation in footprint area of mitochondria for control, LPS challenged and TNF-α challenged cases.

Appendix B: Image Analysis and feature extraction from QPI data

The phase image of the cells extracted from recorded off-axis holograms by writing a MATLAB program for Fourier transform image analysis. The reconstructed phase map of the cells further utilized to extract various parameters to describe the morphology of individual cells. Graphical user interface (GUI) was developed to isolate the cell from the background by putting a threshold value and region of interest (ROI) was selected as shown in figure below. In general the threshold value is set to be the phase sensitivity of the QPI system which is 40 mrad. The phase image of the cell is used as input of the GUI and image is converted in grey image for better boundary detection of cells. Further, the image was segmented by selecting the boundary as depicted in Fig. 11 and various morphological and statistical parameters were extracted from it. The GUI provides the freedom to select a range of mask suitable for the structure and hence useful in exact measurement of the features.

A GUI is developed for the selection cell boundary (i.e. ROI). Following steps are followed to segment the individual cell [51]:

(i) A free hand binary mask is generated to segment the cell from background with the help of expert biologist. The mask only selects region of the cell.

(ii) The pixel's phase values of segmented image below the spatial phase noise level (peak to valley noise value) of the system are set to zero to select only ROI containing cell. This leads to accurate measurement of the phase and subsequently morphological parameters.
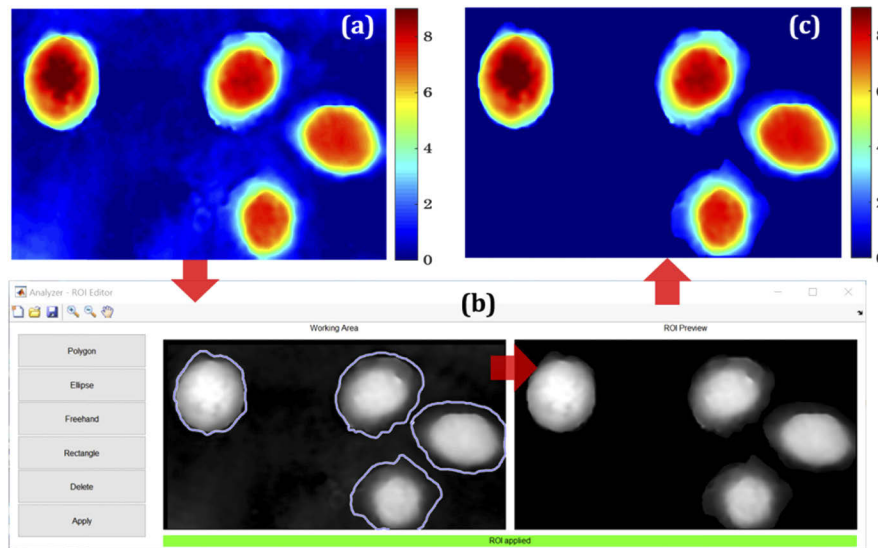
Fig. 11. Graphical user interface developed in MATLAB. Visual presentation of the selection steps for the isolation of the individual cell. (a) Phase map for whole FOV, (b) selection of binary mask to isolate individual cell and segmented cell with threshold value and (c) reconstructed phase map of isolated cells (color bar is in radian).

Appendix C: Visualization of data using t-SNE method

We performed T-SNE method for better visualization of the data plots [49,52]. We have used tsne command in MATLAB R2020a to convert high dimensional data in two-dimension. We have used all default parameters set in tsne command. We have visualized data using 'Mahalanobis' and 'Euclidean' distance metrics to obtain a better separation between data sets. Class 0 corresponds to control state and 1 corresponds to inflammated one. The results of both metrics are shown in Fig. 12.
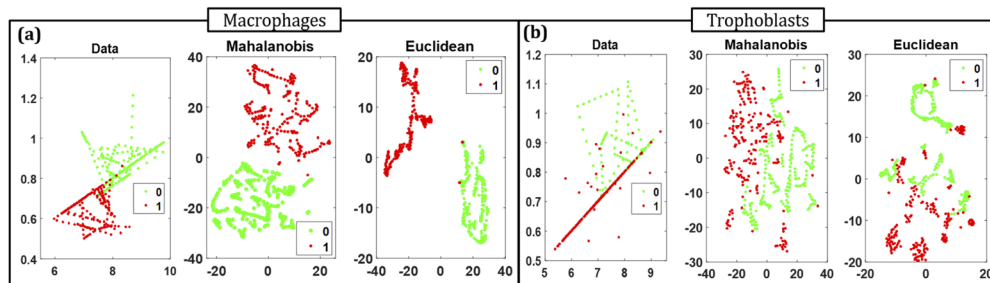
Fig. 12. Data visualization for control and inflammated cells using dimension reduction T-SNE method. Fig. (a) is corresponding to macrophages and (b) is for trophoblasts. The legend 0 is for control state and 1is for inflammated state. Data is well separable using Mahalanobis and Euclidian distance metrics.

It is clear from the figure that data points are well separable for control and inflammated states for both cell lines. Euclidean distance metrics give reasonably good separation of clusters as compared to Mahalanobis distance metric for macrophages as shown in Fig. 12(a). In case of trophoblasts, both the distance metrics having almost similar result (Fig. 12(b)). In conclusion our data set is well separable in t-SNE visualization and having good accuracy for the classification of

control and inflammation states. Also, we have uploaded the raw data on OSA figshare platform in form of excel file corresponding to 400 cells of both cell lines [48].

Disclosures

Authors declare no competing interest.

References

1. B. Chazaud, "Macrophages: supportive cells for tissue repair and regeneration," Immunobiology **219**(3), 172–178 (2014).
2. T. J. Koh and L. A. DiPietro, "Inflammation and wound healing: the role of the macrophage," Expert Rev. Mol. Med. **13**, e23 (2011).
3. J.-L. Mège, V. Mehraj, and C. Capo, "Macrophage polarization and bacterial infections," Curr. Opin. Infect. Dis. **24**(3), 230–234 (2011).
4. J. Van den Bossche, L. A. O'Neill, and D. Menon, "Macrophage immunometabolism: where are we (going)?" Trends Immunol. **38**(6), 395–406 (2017).
5. M. M. Faas and P. De Vos, "Innate immune cells in the placental bed in healthy pregnancy and preeclampsia," Placenta **69**, 125–133 (2018).
6. F. Ning, H. Liu, and G. E. Lash, "The role of decidual macrophages during normal and pathological pregnancy," Am. J. Reprod. Immunol. **75**(3), 298–309 (2016).
7. K. Koga, P. B. Aldo, and G. Mor, "Toll-like receptors and pregnancy: trophoblast as modulators of the immune response," J. Obstet. Gynaecol. Res. **35**(2), 191–202 (2009).
8. J. K. Riley and D. M. Nelson, "Toll-like receptors in pregnancy disorders and placental dysfunction," Clin. Rev. Allergy Immunol. **39**(3), 185–193 (2010).
9. V. Abrahams and G. Mor, "Toll-like receptors and their role in the trophoblast," Placenta **26**(7), 540–547 (2005).
10. G. Mor, S. L. Straszewski-Chavez, and V. M. Abrahams, "Macrophage-trophoblast interactions," in *Placenta and Trophoblast* (Springer, 2006), pp. 149–163.
11. Y. K. Jaiswal, M. K. Jaiswal, V. Agrawal, and M. M. Chaturvedi, "Bacterial endotoxin (LPS)–induced DNA damage in preimplanting embryonic and uterine cells inhibits implantation," Fertil. Steril. **91**(5), 2095–2103 (2009).
12. D.-X. Xu, H. Wang, L. Zhao, H. Ning, Y.-H. Chen, and C. Zhang, "Effects of low-dose lipopolysaccharide (LPS) pretreatment on LPS-induced intra-uterine fetal death and preterm labor," Toxicology **234**(3), 167–175 (2007).
13. A. R. Seminara, P. P. Ruvolo, and F. Murad, "LPS/IFN-γ-Induced RAW 264.7 Apoptosis is Regulated by Both Nitric Oxide–Dependent and–Independent Pathways Involving JNK and the Bcl-2 Family," Cell Cycle **6**(14), 1772–1778 (2007).
14. S. Dröse and U. Brandt, "Molecular mechanisms of superoxide production by the mitochondrial respiratory chain," in *Mitochondrial Oxidative Phosphorylation* (Springer, 2012), pp. 145–169.
15. F. Wu, F. J. Tian, Y. Lin, and W. M. Xu, "Oxidative stress: placenta function and dysfunction," Am. J. Reprod. Immunol. **76**(4), 258–271 (2016).

16. M. P. Murphy, "How mitochondria produce reactive oxygen species," Biochem. J. **417**(1), 1–13 (2009).

17. R. S. Balaban, S. Nemoto, and T. Finkel, "Mitochondria, oxidants, and aging," Cell **120**(4), 483–495 (2005).

18. J. S. Beckman and W. H. Koppenol, "Nitric oxide, superoxide, and peroxynitrite: the good, the bad, and ugly," Am. J. Physiol. Cell Physiol. **271**(5), C1424–C1437 (1996).

19. F. Martínez, M. Kiriakidou, and J. F. Strauss III, "Structural and functional changes in mitochondria associated with trophoblast differentiation: methods to isolate enriched preparations of syncytiotrophoblast mitochondria," Endocrinology **138**(5), 2172–2183 (1997).

20. D. D. L. R. Castillo, M. Zarco-Zavala, S. Olvera-Sanchez, J. P. Pardo, O. Juarez, F. Martinez, G. Mendoza-Hernandez, J. J. García-Trejo, and O. Flores-Herrera, "Atypical cristae morphology of human syncytiotrophoblast mitochondria role for complex V," J. Biol. Chem. **286**(27), 23911–23919 (2011).

21. M. G. Gustafsson, "Surpassing the lateral resolution limit by a factor of two using structured illumination microscopy," J. Microsc. **198**(2), 82–87 (2000).

22. B. O. Leung and K. C. Chou, "Review of super-resolution fluorescence microscopy for biology," Appl. Spectrosc. **65**(9), 967–980 (2011).

23. I. S. Opstad, D. L. Wolfson, C. I. Øie, and B. S. Ahluwalia, "Multi-color imaging of sub-mitochondrial structures in living cells using structured illumination microscopy," Nanophotonics **7**(5), 935–947 (2018).

24. L. Shao, P. Kner, E. H. Rego, and M. G. Gustafsson, "Super-resolution 3D microscopy of live whole cells using structured illumination," Nat. Methods **8**(12), 1044–1046 (2011).

25. M. Mir, B. Bhaduri, R. Wang, R. Zhu, and G. Popescu, "Quantitative phase imaging," Prog. Opt. **57**, 133–217 (2012).

26. K. Lee, K. Kim, J. Jung, J. Heo, S. Cho, S. Lee, G. Chang, Y. Jo, H. Park, and Y. Park, "Quantitative phase imaging techniques for the study of cell pathophysiology: from principles to applications," Sensors **13**(4), 4170–4191 (2013).

27. V. Dubey, D. Popova, A. Ahmad, G. Acharya, P. Basnet, D. S. Mehta, and B. S. Ahluwalia, "Partially spatially coherent digital holographic microscopy and machine learning for quantitative analysis of human spermatozoa under oxidative stress condition," Sci. Rep. **9**(1), 3564 (2019).

28. A. Ahmad, V. Dubey, G. Singh, V. Singh, and D. S. Mehta, "Quantitative phase imaging of biological cells using spatially low and temporally high coherent light source," Opt. Lett. **41**(7), 1554–1557 (2016).

29. V. Dubey, A. Ahmad, R. Singh, D. L. Wolfson, P. Basnet, G. Acharya, D. S. Mehta, and B. S. Ahluwalia, "Multi-modal chip-based fluorescence and quantitative phase microscopy for studying inflammation in macrophages," Opt. Express **26**(16), 19864–19876 (2018).

30. N. T. Shaked, M. T. Rinehart, and A. Wax, "Dual-interference-channel quantitative-phase microscopy of live cell dynamics," Opt. Lett. **34**(6), 767–769 (2009).

31. G. Popescu, T. Ikeda, C. Best, K. Badizadegan, R. R. Dasari, and M. S. Feld, "Erythrocyte structure and dynamics quantified by Hilbert phase microscopy," J. Biomed. Opt. **10**(6), 060503 (2005).

32. V. K. Lam, T. C. Nguyen, V. Bui, B. M. Chung, L.-C. Chang, G. Nehmetallah, and C. B. Raub, "Quantitative scoring of epithelial and mesenchymal qualities of cancer cells using machine learning and quantitative phase imaging," J. Biomed. Opt. **25**(2), 026002 (2020).

33. Y. Ozaki, H. Yamada, H. Kikuchi, A. Hirotsu, T. Murakami, T. Matsumoto, T. Kawabata, Y. Hiramatsu, K. Kamiya, and T. Yamauchi, "Label-free classification of cells based on supervised machine learning of subcellular structures," PLoS One **14**(1), e0211347 (2019).

34. M. N. Wernick, Y. Yang, J. G. Brankov, G. Yourganov, and S. C. Strother, "Machine learning in medical imaging," IEEE Signal Process. Mag. **27**(4), 25–38 (2010).

35. Y. Liu, "Active learning with support vector machine applied to gene expression data for cancer classification," J. Chem. Inf. Model. **44**(6), 1936–1941 (2004).

36. D. Giustarini, R. Rossi, A. Milzani, and I. Dalle-Donne, "Nitrite and nitrate measurement by Griess reagent in human plasma: evaluation of interferences and standardization," Methods Enzymol. **440**, 361–380 (2008).

37. K. Schulz, S. Kerber, and M. Kelm, "Reevaluation of the Griess method for determining NO/NO− 2 in aqueous and protein-containing samples," Nitric Oxide **3**(3), 225–234 (1999).

38. A. Ahmad and D. S. Mehta, "Quantitative Phase Microscopy and Tomography with Spatially Incoherent Light," Advances in Optics: Reviews. Book Series **3**, 487–511 (2018).

39. B. S. Penatti, M. D. B. Battistella, M. T. da Silva, N. F. Rosa, S. R. Chvaicer, A. P. de Almeida Righi, L. Ferraz, A. M. de Oliveira Jucá, R. G. dos Reis Guidoni, and T. Q. Penati, "95 Nitric oxide in preeclampsia: Clinical correlations and serum levels: Biomarkers, prediction of preeclampsia," Pregnancy Hypertension: An International Journal of Women's Cardiovascular Health **6**(3), 224–225 (2016).

40. U. Von Mandach, D. Lauth, and R. Huch, "Maternal and fetal nitric oxide production in normal and abnormal pregnancy," J. Matern.-Fetal Neonat. Med. **13**(1), 22–27 (2003).

41. A. Aris, S. Benali, A. Ouellet, J. Moutquin, and S. Leblanc, "Potential biomarkers of preeclampsia: inverse correlation between hydrogen peroxide and nitric oxide early in maternal circulation and at term in placenta of women with preeclampsia," Placenta **30**(4), 342–347 (2009).

42. M. J. Kupferminc, A. M. Peaceman, T. R. Wigton, K. A. Rehnberg, and M. L. Socol, "Tumor necrosis factor-α is elevated in plasma and amniotic fluid of patients with severe preeclampsia," Am. J. Obstet. Gynecol. **170**(5), 1752–1759 (1994).

43. O. Arican, M. Aral, S. Sasmaz, and P. Ciragil, "Serum levels of TNF-α, IFN-γ, IL-6, IL-8, IL-12, IL-17, and IL-18 in patients with active psoriasis and correlation with disease severity," Mediators Inflammation **2005**(5), 273–279 (2005).

44. T. Guzik, R. Korbut, and T. Adamek-Guzik, "Nitric oxide and superoxide in inflammation," Can. J. Physiol. Pharmacol. **54**, 469–487 (2003).

45. R. Korhonen, A. Lahti, H. Kankaanranta, and E. Moilanen, "Nitric oxide production and signaling in inflammation," Curr. Drug Targets: Inflammation Allergy **4**(4), 471–479 (2005).

46. A. J. Valente, L. A. Maddalena, E. L. Robb, F. Moradi, and J. A. Stuart, "A simple ImageJ macro tool for analyzing mitochondrial network morphology in mammalian cell culture," Acta Histochem. **119**(3), 315–326 (2017).

47. J. Jonkman, C. M. Brown, G. D. Wright, K. I. Anderson, and A. J. North, "Tutorial: guidance for quantitative confocal microscopy," Nat. Protoc. **15**(5), 1585–1611 (2020).

48. 10.6084/m9.figshare.12278747.

49. L. v. d. Maaten and G. Hinton, "Visualizing data using t-SNE," J. Mach. Learn. Res. **9**, 2579–2605 (2008).

50. J.-Y. Lee and M. Kitaoka, "A beginner's guide to rigor and reproducibility in fluorescence imaging experiments," Mol. Biol. Cell **29**(13), 1519–1525 (2018).

51. S. T. Smith, *MATLAB: Advanced GUI Development* (Dog Ear Publishing, 2006).

52. L. van der Maaten and G. Hinton, "User's Guide for t-SNE Software," Structure (2008).